namely a fall of about 1.0 p.p.m. in capacitance over the temperature range used. The agreement between the two sets of data, taken in separate runs a few months apart, shows that the capacitor behaves reproducibly at a level of one in 10^7 over a long time period.

Knowing the background capacitance, we can investigate the effect of the quantum exclusion. The measured change in capacitance for a 0.1% ^{3}He in ^{4}He solution with the background subtracted is shown in Fig. 2 inset. The main graph in Fig. 2 shows the data converted to ^{3}He filling factor in the pores, defined as the ratio of ^{3}He concentration in the pores to total ^{3}He concentration in the solution—that is, complete penetration of ^{3}He into the pores corresponds to a filling factor of unity. The conversion requires no adjustable parameters as we know all the volumes in the cell. Figure 2 shows that the filling factor in the pores has increased by 0.2 over our temperature range. The effect of the quantum exclusion with the gradual expulsion of ^{3}He from the confined region as the temperature falls is quite clear. Had we been able to work at a lower temperature and with a concentration approaching the ideal situation of Fig. 1, we should have been able to span a temperature range where the filling factor changed from near zero to unity—that is, from complete exclusion to complete penetration.

We can compare the observed ^{3}He penetration with a calculation made on the basis of a simple single-particle model. Although Vycor glass has a complicated structure, for a zeroth-order model we assume the pores to constitute an array of uniform quantum wires with a square cross-section of width a and with the known total volume. The ^{3}He density of states is then given by the combination of transverse standing-wave states in the square cross-section and the free longitudinal motion. This gives a density of states as a function of energy ϵ made up of a number of $(\epsilon - \epsilon_0)^{-1/2}$ terms in which $\epsilon_0 = (n^2 + l^2)E_0/2$ with $E_0 = h^2/4m^*a^2$, and where n and l are the positive integer quantum numbers defining the transverse state. (The two lowest such terms are those shown in Fig. 1.)

This calculation has just one adjustable parameter, the confinement energy E_0, or equivalently the channel width a. We note that a here is the width open to ^{3}He quasiparticles; this is the bare Vycor channel width minus ~1 nm to allow for the two atomic layers of solid ^{4}He adsorbed on the wall. The density of states so derived may be directly compared with the experiment because there are no other unknowns. We assume that the states are filled with the Fermi Dirac distribution, and compute the chemical potential needed to ensure that the correct total number of ^{3}He quasiparticles occupies the cell. The three curves in Fig. 2 show the filling factor calculated in this way on the assumption that $a = 7$, 10, 12 nm, that is, that $E_0 = 5$, 7.5, 15 mK. Given the simplicity of the assumptions, the agreement between the observed filling factor and the quantum exclusion calculation for $a \approx 10$ nm is good over the whole temperature range.

This agreement confirms that there is indeed a change in the quantum confinement of ^{3}He quasiparticles in narrow channels as a function of temperature. This is, to our knowledge, the first confinement experiment to be performed in helium; with more refined techniques we expect to gain access to a whole range of mesoscopic behaviour which has no analogue in electronic systems. For example, the equivalent of the metal/insulator transition near the critical point is complicated in the charged system by the Coulombic repulsion between the electrons. It would also be interesting to study more dilute solutions and/or narrower channels where E_F could be adjusted to be much smaller than the confinement energy, as with low enough temperatures we would see the complete transition from exclusion to penetration. Finally, we could add an energy ~±10 mK to the confinement energy by applying a high magnetic field, making the quantum exclusion from the channels dependent on the quasiparticle spin. This would greatly enhance the effect for the antiparallel spin, and suggests that a porous membrane in a high magnetic field might provide a ^{3}He polarization filter[5]. □

Received 28 May; accepted 27 July 1998.

1. Sohn, L. L., Kouwenhoven, L. P. & Schön, G. (eds) *Mesoscopic Electron Transport* (NATO ASI Ser, Vol. 345, Kluwer Academic, 1997).
2. Owers-Bradley, J. R. Spin-polarized ^{3}He-^{4}He liquids. *Rep. Prog. Phys.* **60,** 1173–1216 (1998).
3. Levitz, P., Ehret, G., Sinha, S. K. & Drake, J. M. Porous vycor glass—the microstructure as probed by electron microscopy, direct energy transfer, small angle scattering, and molecular adsorption. *J. Chem. Phys.* **95,** 6151–6161 (1991).
4. Bunkov, Yu. M. *et al.* A compact dilution refrigerator with vertical heat exchangers for operation to 2 mK. *J. Low Temp. Phys.* **83,** 257–272 (1991).
5. Ohi, A. & Nakayama, T. Percolative diffusion of dissolved ^{3}He atoms in He II through porous media. *J. Low Temp. Phys.* **81,** 349–368 (1990).
6. Kierstead, H. A. Dielectric constant, molar volume, and phase diagram of saturated ^{3}He-^{4}He mixtures. *J. Low Temp. Phys.* **24,** 497–512 (1976).
7. Castelijns, C. A. M., Kuerten, J. G. M., de Waele, A. T. A. M. & Gijsman, H. M. ^{3}He flow in dilute ^{3}He-^{4}He mixtures at temperatures between 10 and 150 mK. *Phys. Rev. B* **52,** 2870–2886 (1985).

Acknowledgements. We thank V. Fal'ko and A. Volkov for discussions.

Correspondence and requests for materials should be addressed to A.M.G. (e-mail: a.guenault@lancaster.ac.uk).

Spin fluctuations in $YBa_2Cu_3O_{6.6}$

H. A. Mook*, Pengcheng Dai*, S. M. Hayden†, G. Aeppli‡, T. G. Perring§ & F. Doğan‖

* *Oak Ridge National Laboratory, Oak Ridge, Tennessee 37831-6393, USA*
† *H. H. Wills Physics Laboratory, University of Bristol, Bristol BS8 1TL, UK*
‡ *NEC Research Institute, 4 Independence Way, Princeton, New Jersey 08540, USA*
§ *ISIS Facility, Rutherford Appleton Laboratory, Chilton, Didcot OX11 0QX, UK*
‖ *Department of Materials Sciences and Engineering, University of Washington, Seattle, Washington 98195, USA*

An important feature of the high-transition-temperature (high-T_c) copper oxide superconductors is the magnetism that results from the spins associated with the incomplete outer electronic shells ($3d^9$) of the copper ions. Fluctuations of these spins give rise to magnetic excitations of the material, and might mediate the electron pairing that leads to superconductivity. If the mechanism for high-T_c superconductivity is the same for all copper oxide systems, their spin fluctuations should be universal. But so far, the opposite has seemed to be the case: neutron scattering data reveal clear differences between the spin fluctuations for two major classes of high-T_c materials, $La_{2-x}Sr_xCuO_4$ (refs 1–3) and $YBa_2Cu_3O_{7-x}$ (refs 4–6), whose respective building blocks are CuO_2 layers and bilayers. Here we report two-dimensional neutron-scattering imaging of $YBa_2Cu_3O_{6.6}$, which reveals that the low-frequency magnetic excitations are virtually identical to those of similarly doped $La_{2-x}Sr_xCuO_4$. Thus, the high-temperature ($T_c \lesssim 92$ K) superconductivity of the former materials may be related to spatially coherent low-frequency spin excitations that were previously thought to be unique to the lower-T_c (<40 K) single-layer $La_{2-x}Sr_xCuO_4$ family.

The most celebrated common feature of copper oxide magnetism is that the undoped parent compounds are insulating antiferromagnets, characterized by a simple doubling of the crystallographic unit cells in the CuO_2 planes. Neutron scattering, which measures the Fourier transform (in space and time) of the spin–spin correlation function, long ago imaged the doubling[7,8] that manifests itself in diffraction peaks at the wavevectors (1/2, 1/2). To label wavevectors in two-dimensional reciprocal space (Fig. 1a), we use reciprocal lattice units such that (1,0) and (0,1) are along the nearest-neighbour copper–oxygen–copper paths and are the locations of the lowest-order diffraction peaks from the nuclei in the nearly square CuO_2 planes. Upon chemical doping to induce metallic and superconducting behaviours, the elastic diffraction peaks, due to static magnetic order, disappear. Both antiferromagnetic and superconducting compositions show strong inelastic scattering derived from magnetic fluctuations. For superconducting

Nature © Macmillan Publishers Ltd 1998

$La_{2-x}Sr_xCuO_4$ (214), the low-frequency inelastic scattering peaks are not at (1/2, 1/2), but at a quartet of nearby incommensurate wavevectors (indicated in Fig. 1a). As a function of frequency, no particularly sharp features have been identified. Chemical doping can be achieved by substitution of Sr, Ba or Ca for La or by intercalation of excess oxygen. The details of the scattering depend only on the unbound charge introduced by the dopants, and not on the method for introducing the charge[9]. For $YBa_2Cu_3O_{7-x}$ (123), which so far has only been doped by excess oxygen, the inelastic scattering was thought to be dominated by broader maxima still centred at (1/2, 1/2). Furthermore, when frequency is scanned, the scattering displays a sharp resonance whose position varies with T_c (refs 10, 11). Dai *et al.* have recently shown that for $YBa_2Cu_3O_{6.6}$ ($T_c = 62.7$ K), the situation is more complex[12]. Even though there is a sharp resonance centred at 34 meV and peaking at (1/2, 1/2), the lower-frequency spin fluctuations actually peak away from (1/2, 1/2). Because of experimental limitations, Dai *et al.*[12] were unable to determine either the precise displacements of the peaks from (1/2, 1/2) or the absolute amplitudes characterizing the fluctuations. A breakthrough in experimental technology, namely the two-dimensional position-sensitive detection of scattered neutrons in the High Energy Transfer time-of-flight neutron spectrometer at ISIS, the most powerful pulsed spallation neutron source, has now allowed us to image the fluctuations in the same 25.6-g sample. The outcome is a quantitative resolution of the issues left unresolved by Dai *et al.*[12] which permits direct comparison with (214) materials.

To our knowledge, these data are the first maps of the magnetic scattering ever produced in the two-dimensional reciprocal space for the CuO_2 planes in (123). As the experiments are time-consuming (Fig. 1 legend), we chose two measuring frequencies. The first is 34 ± 2 meV, where the resonance for this particular doping level occurs. Figure 1b and c illustrates the outcome at 13 K and 65 K ($T_c + 2.3$ K). In agreement with previous measurements[10,11], which were one-dimensional cuts through this map, there is a broad peak

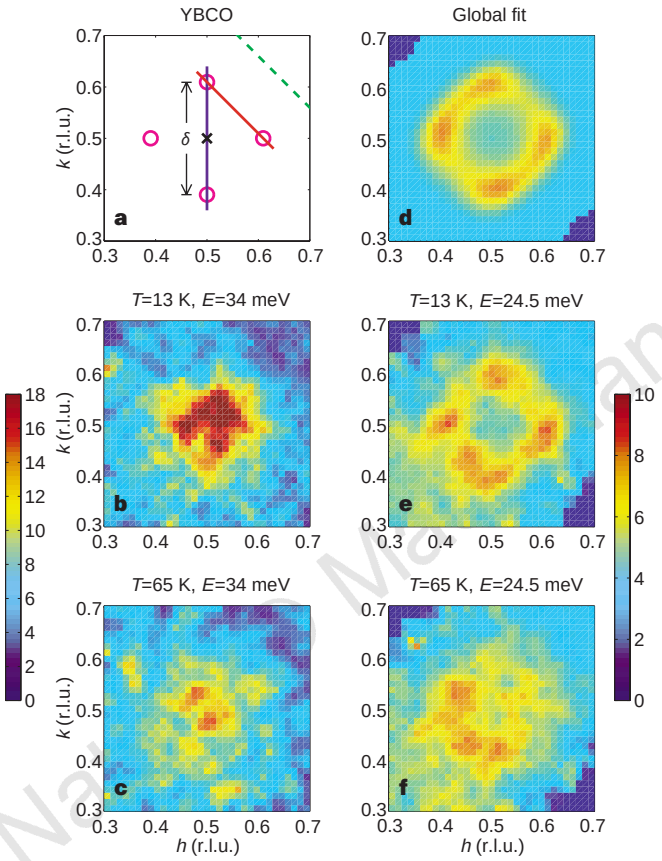

Figure 1 Reciprocal lattice diagram and neutron-scattering results. **a**, Two-dimensional reciprocal space for the CuO_2 planes in the cuprates. The cross marks the (1/2, 1/2) point at which magnetic Bragg scattering appears in the parent insulating compounds; the quartet of circles indicates the locus of magnetic intensity maxima in the superconductors measured in reciprocal lattice units (r.l.u.). **b**, Image of the 34 meV resonance at 13 K for $YBa_2Cu_3O_{6.6}$. The crystal and neutron-scattering instrument are three-dimensional, so that we are observing a two-dimensional cut through reciprocal space, with the out-of-plane wavevector component integrated from $(\pi/d)(1-0.5)$ to $(\pi/d)(1+0.5)$ where $d = 3.342$ Å, the interlayer spacing. The colour bar gives intensities in the absolute units of mbarn sr^{-1} meV^{-1} F.U.$^{-1}$. **c**, Image at the resonance frequency on warming to 65 K. **e**, **f**, Images of the subresonance (24 meV) scattering at 13 and 65 K, respectively; **d**, image that is the convolution of a four-fold symmetric, noise-free model function, similar to those used previously[13] on incommensurate spin fluctuations in (214) and the response function of the instrument. The energy probed increases on moving diagonally (from bottom left) across the images, with the incommensurate peaks in **e** appearing at 22 and 26 meV. The counting times required to collect the images were 12, 16, 114, 63 h for images **b**, **c**, **e**, **f**, respectively, with the proton current of 170 μA. The scattering was placed on an absolute scale using the elastic incoherent scattering from a vanadium standard under the same experimental conditions (see refs 16, 17, for example).

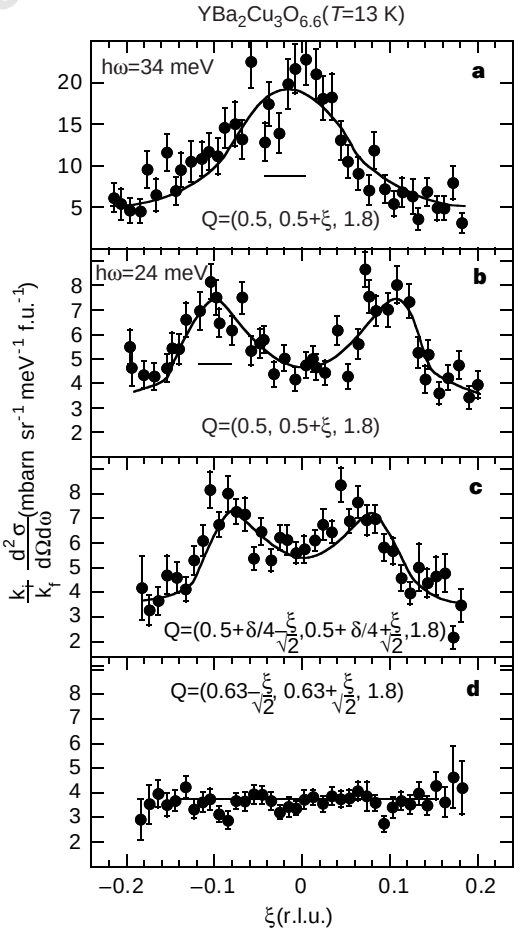

Figure 2 Data obtained from cuts through the two-dimensional images in Fig. 1. **a**, Data obtained along (0,1) through the low-temperature resonance maximum at (1/2, 1/2) and 34 meV. **b–d**, Data obtained from cuts through the low-temperature incommensurate pattern. The coloured lines in Fig. 1a show the direction of the cuts. **b–d**, Data from cuts taken **b**, vertically through the corners of the square, and **c**, along the square edge; **d**, background. Solid lines are derived similarly from the model image in Fig. 1d. Horizontal bars represent the full-width at half-maximum of the experimental resolution function.

Nature © Macmillan Publishers Ltd 1998

Nature © Macmillan Publishers Ltd 1998

Table 1 Comparison of parameters derived from neutron scattering data

Compound	Ref.	x	T (K)	Energy (meV)	δ (r.l.u.)	κ_ω (Å^{-1})	$\chi''(\omega)$ (μ_B^2 eV^{-1} Cu^{-1})
La_2CuO_4	16	0	295	20	0		1.5 ± 0.5
$YBa_2Cu_3O_{6.2}$	17	0	295	24	0		1.8 ± 0.4
$La_{1.9}Sr_{0.1}CuO_4$	14	0.1	8	8	0.21 ± 0.02	0.038 ± 0.005	
$YBa_2Cu_3O_{6.6}$		0.1	13	24	0.21 ± 0.02	0.041 ± 0.005	2.5 ± 0.5
$La_{1.86}Sr_{0.14}CuO_4$	13, 16	0.14	35	15	0.24 ± 0.004	0.052 ± 0.002	4 ± 1
$YBa_2Cu_3O_{6.6}$		0.1	13	34	0		9.5 ± 2

x is the hole doping expressed in the units of electrons per planar Cu atom, δ the incommensurability parameter in reciprocal lattice units, κ_ω the half-width at half-maximum of the incommensurate peaks which reflects the inverse correlation length (related to but not equal to $\kappa(\omega)$ in ref. 13), and $\chi''(\omega)$ the wavevector-integrated susceptibility. Reference 14 defines δ as a factor of 2 smaller. The wavevector-integrated susceptibility is expressed per planar Cu.

centred at (1/2, 1/2) which, although it is already present at T_c, grows substantially on cooling into the superconducting state.

Figure 1e and f shows the dramatically different patterns obtained at 24.5 ± 2.5 meV: frame e reveals that the scattering at 13 K essentially disappears at (1/2, 1/2) and acquires maxima at the four positions displaced by (0, ±δ/2) and (±δ/2, 0) from (1/2, 1/2)—the orientation of the pattern is clearly the same as for (214); frame f shows a measurement at 65 K that demonstrates that the pattern is broader at the higher temperature. In Fig. 2 we plot cuts through the maps along the lines shown in Fig. 1a. What emerges again is that the 24-meV low-temperature scattering can be visualized as a square box with subsidiary maxima at the corners and relatively little scattering at the commensurate position (1/2, 1/2). The intensities are given as absolute scattering cross-sections and the solid lines are from a global fit to the same model used previously to analyse (214) neutron-scattering results[13]. A slight modification of the formalism was included which allows for an anisotropic peak shape and results in a better fit. Figure 1d shows how the fitting function appears in the two-dimensional reciprocal space for the CuO_2 planes.

Scattering identified as stemming from the lattice vibrations (phonons) with energies near 20 meV is visible in the lower left part of the pattern in Fig. 1f. Some phonon scattering is also apparent at low temperatures, but it does not alter the shape of the pattern from the magnetic scattering. The present experiment is unique not only for its use of two-dimensional position-sensitive detection, but also because of its small phonon background. In particular, the evacuated and obstruction-free flight paths of the instrument permitted data collection at low scattering angles, resulting in low neutron momentum transfer, Q. Minimizing Q is the most efficient way to minimize phonon and multiphonon scattering, whose power varies as Q^2 and Q^4, respectively. Although earlier experiments have looked near wavevectors such as (1/2, 3/2)—equivalent to (1/2, 1/2)—the actual net neutron momentum transfer has generally been ~2.73 Å^{-1}, whereas here $Q \approx 1.47$ Å^{-1}.

Table 1 lists parameters not only for our (123) sample at the two energy values probed, but also for (214) crystals examined previously. Parameters determined from the scattering patterns are the peak positions δ, the inverse coherence length κ_ω, given by the width of the features in the pattern, and the wavevector-integrated spectral weight $\chi''(\omega)$. Several conclusions emerge from Table 1, the most important being that the wavevectors for the incommensurate fluctuations in Fig. 1 are indistinguishable from those for similarly doped[14] single-layer (214) materials[1,15]. In addition, the coherence lengths of the incommensurate excitations are similar for similar doping levels and energy transfers scaled by T_c in the (214) and (123) materials. Furthermore, the integrated intensities of the incommensurate peaks, when measured at the same scaled energies, are also comparable[16]. They are also not far from the integrated spin wave intensities, measured at the same energies for the undoped antiferromagnetic parent compounds[17]. In contrast, the resonance in (123) is substantially more intense than the spin waves. A final point of resemblance between the spin fluctuations in (123) and (214) is that cooling into the superconducting phase appears to narrow the incommensurate peaks, and thus increases the magnetic coherence. In our experiment, this effect is most clearly manifested by the poorer definition of the low-intensity 'hole' around (1/2, 1/2) at 65 K (Fig. 1f) compared with at 13 K (Fig. 1e); in previous work on slightly differently doped (214), it made itself apparent in better defined, enhanced incommensurate peaks[18].

We have discovered that for the same hole doping, the low-frequency, subresonance, magnetic fluctuations in $(123)O_{6.6}$ are remarkably similar to those in superconducting (214). Not only are their wavevectors and coherence lengths essentially the same, but their spectral weights are comparable. Furthermore, the fluctuations in both compounds share the phenomenon of increased coherence in the superconducting phase. The consequences for our understanding of the copper oxide superconductors are clear—the magnetic fluctuations at low frequencies are beginning to achieve the same universality across widely different materials with different values of T_c, which characterizes many of their macroscopic properties. As for the bulk characteristics, the controlling factor seems only to be the hole density. Thus all electronic structure, and other detailed effects not connected with CuO_2 planes with a particular carrier density, appears to drop out at low frequencies, even for short-wavelength spin fluctuations. This represents a huge simplification of the high-T_c problem and was not obvious from previous magnetic resonance, magnetic susceptibility, and neutron data. □

Received 29 April; accepted 2 July 1998.

1. Cheong, S.-W. *et al.* Incommensurate magnetic fluctuations in $La_{2x}Sr_xCuO_4$. *Phys. Rev. Lett.* **67,** 1791–1794 (1991).
2. Mason, T. E., Aeppli, G. & Mook, H. A. Magnetic dynamics of superconducting $La_{1.86}Sr_{0.14}CuO_4$. *Phys. Rev. Lett.* **68,** 1414–1417 (1992).
3. Thurston, T. R. *et al.* Low-energy incommensurate spin excitations in superconducting $La_{1.85}Sr_{0.15}CuO_4$. *Phys. Rev. B* **46,** 9128–9131 (1992).
4. Rossat-Mignod, J. *et al.* Neutron scattering study of the $YBa_2Cu_3O_{6+x}$ system. *Physica* **185 C,** 86–92 (1991).
5. Tranquada, J. M., Gehring, P. M., Shirane, G., Shamoto, S. & Sato, M. Neutron-scattering study of the dynamical spin susceptibility in $YBa_2Cu_3O_{6.6}$. *Phys. Rev. B* **46,** 5561–5575 (1992).
6. Sternlieb, B. J., Tranquada, J. M., Shirane, G., Sato, M. & Shamoto, S. **q** dependence of the dynamic susceptibility $\chi''(\mathbf{q}, \omega)$ in superconducting $YBa_2Cu_3O_{6.6}$ ($T_c = 46$ K). *Phys. Rev. B* **50,** 12915–12919 (1994).
7. Vaknin, D. *et al.* Antiferromagnetism in La_2CuO_{4-y}. *Phys. Rev. Lett.* **58,** 2802–2805 (1987).
8. Tranquada, J. M. *et al.* Neutron-diffraction determination of antiferromagnetic structure of Cu ions in $YBa_2Cu_3O_{6+x}$ with $x = 0.0$ and 0.15. *Phys. Rev. Lett.* **60,** 156–159 (1988).
9. Wells, B. O. *et al.* Incommensurate spin fluctuations in high-transition temperature superconductors. *Science* **277,** 1067–1071 (1997).
10. Dai, P., Yethiraj, M., Mook, H. A., Lindemer, T. B. & Doğan, F. Magnetic dynamics in underdoped $YBa_2Cu_3O_{7-x}$: direct observations of a superconducting gap. *Phys. Rev. Lett.* **77,** 5425–5428 (1996).
11. Fong, H. F., Keimer, B., Milius, D. L. & Aksay, I. A. Superconducting-induced anomalies in the spin excitation spectra of underdoped $YBa_2Cu_3O_{6+x}$. *Phys. Rev. Lett.* **78,** 713–716 (1997).
12. Dai, P., Mook, H. A. & Doğan, F. Incommensurate magnetic fluctuations in $YBa_2Cu_3O_{6.6}$. *Phys. Rev. Lett.* **80,** 1738–1741 (1998).
13. Aeppli, G., Mason, T. E., Hayden, S. M., Mook, H. A. & Kulda, J. Nearly singular magnetic fluctuations in the normal state of a high-T_c cuprate superconductor. *Science* **278,** 1432–1435 (1997).
14. Yamada, K. *et al.* Doping dependence of the spatially modulated dynamical spin correlations and the superconducting-transition temperature in $La_{2-x}Sr_xCuO_4$. *Phys. Rev. B* **57,** 6165–6172 (1998).
15. Tallon, J. L., Bernhard, C., Shaked, H., Hitterman, R. L. & Jorgensen, J. D. Generic superconducting phase behavior in high-T_c cuprates: T_c variation with hole concentration in $YBa_2Cu_3O_{7-x}$. *Phys. Rev. B* **51,** 12911–12914 (1995).
16. Hayden, S. M. *et al.* Comparison of the high-frequency magnetic fluctuations in insulating and superconducting $La_{2-x}Sr_xCuO_4$. *Phys. Rev. Lett.* **76,** 1344–1347 (1996).
17. Hayden, S. M., Aeppli, G., Perring, T. G., Mook, H. A. & Doğan, F. High-frequency spin waves in $YBa_2Cu_3O_{6.15}$. *Phys. Rev. B* **54,** R9605–R6908 (1996).
18. Mason, T. E., Schröder, A., Aeppli, G., Mook, H. A. & Hayden, S. M. New magnetic coherence effect in superconducting $La_{2-x}Sr_xCuO_4$. *Phys. Rev. Lett.* **77,** 1604–1607 (1996).

Acknowledgements. We thank R. Coldea, D. A. Tennant, C. Frost and T. B. Lindemer for technical assistance. Support at Oak Ridge was received from the US DOE.

Correspondence and requests for materials should be addressed to H.A.M. (e-mail: ham@ornl.gov).

Nature © Macmillan Publishers Ltd 1998